Polymorphic crystallization of interface stabilized amorphous Fe-Zr thin films under variable driving force

U. Herr, H. Geisler, H. Ippach, and K. Samwer
Institute of Physics, University of Augsburg, D-86135 Augsburg, Germany
(Received 22 September 1998)

We report about experiments concerning the stability of thin films of $Fe_{100-x}Zr_x$ in the concentration range $0<x<7$ at. %. The films are grown using electron beam evaporation under UHV conditions on Zr base layers at 300 K. On these substrate layers, pure Fe and the Fe-Zr alloy films initially grow in the amorphous phase. At a critical thickness d_c, crystallization of the films is observed at room temperature. The crystallization is monitored quantitatively using the magnetic properties of the Fe-Zr alloys which are paramagnetic at room temperature in the amorphous state but ferromagnetic in the bcc phase. The thickness d_c increases with increasing Zr concentration from about 2 nm for pure Fe to 30 nm for $x=7$ at. %. A model for the transformation of the amorphous layer is presented which includes the variation of the thermodynamic driving force with the Zr concentration and the stabilizing effect of the interface to the Zr substrate layer. The model can account for the concentration dependence of d_c and yields a reasonable value for the interface energy contributions. Additional contributions to the phase stabilities such as elastic energy and defect contributions will modify the energy balance between driving force and interface stabilization and may therefore influence the transformation. A quantitative treatment shows that contributions from grain boundaries formed during the crystallization have to be considered whereas the elastic energy contributions are less important. This is a consequence of the large driving forces for polymorphous crystallization. The results are not unique to the Fe-Zr system but should also apply to other Fe–early transition metal or Fe–rare-earth multilayers. [S0163-1829(99)00921-2]

I. INTRODUCTION

It is well known that on suitable substrates which often have the same crystal structure as the desired nonequilibrium phase or at least a common set of lattice planes, it is possible to induce growth of metastable phases. An example is the epitaxial growth of fcc Fe on fcc Cu substrates where both elements have very similar atomic sizes.[1,2] The lower interface energy of the coherent fcc-fcc interface in comparison with the higher energy of the incoherent fcc Cu–bcc Fe interface is the reason for the formation of the fcc Fe which would otherwise occur only at high temperatures. Another example is the formation of bcc Co in thin films grown on (001) GaAs.[3]

In the past years, it has been observed that Fe grows in the amorphous modification on suitable substrates. These substrates are usually early transition elements like Y,[4] Zr,[5] or rare earth elements such as Ce,[6,7] or Gd.[8] In all cases there is a large atomic size mismatch between substrate and Fe atoms hindering epitaxial growth. If grown on other substrates such as Cu,[1,2] or Ag,[9,10] Fe films of comparable thickness grow in the crystalline state.

The amorphous Fe is easily identified in these experiments due to its magnetic properties: amorphous Fe films grown under these conditions are paramagnetic at room temperature and exhibit magnetic ordering only at low temperatures. Mössbauer spectroscopy and magnetization measurements can therefore not only distinguish between the amorphous and the bcc Fe but also quantify the amounts of phases present due to their magnetic signatures.

In the earlier studies[4–8] it has been found that the amorphous Fe phase is only stable at small film thicknesses. If the thickness exceeds a critical value which is about 1.6–2.3 nm in all the experiments, crystallization sets in. Upon crystallization, most of the initially amorphous layer transforms into bcc Fe. The almost complete crystallization shows that the formation of the amorphous phase is not caused by an interdiffusion reaction. In the case of an interdiffusion reaction [SSAR (Ref. 11)] the formation of the amorphous phase would be caused by the supersaturation of the Fe with the rare earth or early transiton element which would be irreversible due to the large negative heat of mixing. In this case, there would be no driving force for polymorphous crystallization of the alloy but the crystallization would require diffusive phase separation.

The experimental work presented here is motivated by the idea that the amorphous Fe in the multilayers is stablized by the low energy of the film-substrate interface. Since the small critical thickness which is only about 10 times the (110) lattice spacings of bcc Fe makes it difficult to distinguish between effects of interface energy contributions and intermixing, we conducted a series of experiments on $Fe_{100-x}Zr_x$ films with $0\leqslant x\leqslant 7$ at. %. The idea behind the use of an alloy system instead of pure Fe layers is to reduce the driving force for crystallization of the $Fe_{100-x}Zr_x$ and thereby extend the range of conditions under which the amorphous phase can be obtained. For $x>7$ at. %, $Fe_{100-x}Zr_x$ films grow in the amorphous phase for all thicknesses.[12,13]

The paper is organized as follows. We will first give a description of the experimental conditions and characterize the samples using x-ray diffraction and magnetic properties.

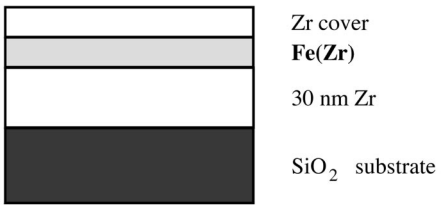

FIG. 1. Schematic cross section through the $Zr/Fe_{100-x}Zr_x/Zr$ multilayer.

The composition profile across the interface is studied by x-ray reflectivity measurements. The crystallization of $Fe_{100-x}Zr_x$ layer in the composition range $0 \leqslant x \leqslant 7$ at. % is studied both *ex situ* and *in situ* during sample preparation (using RHEED and MOKE measurements). It is found that the critical thickness d_c for the crystallization increases with increasing Zr concentration x. A model for the crystallization process is presented and the contributions of chemical and elastic energies are discussed. The model can explain the observed concentration dependent crystallization behavior and yields quantitative information about the interface stabilization effect. The uncertainties of this value are discussed taking into account other possible contributions to the phase stabilities.

II. EXPERIMENT

The samples have been prepared by electron beam evaporation under UHV conditions ($p \leqslant 10^{-9}$ Torr). The Fe-Zr solid solutions have been deposited by simultaneous evaporation from separate sources onto thermally oxidized (001) oriented Si wafers at a temperature of 300 K. Evaporation rates were controlled by individual quartz thickness monitors for each evaporator. The experimental setup is described in detail in Ref. 14. A schematic cross section of the samples is shown in Fig. 1. For *ex situ* characterization outside the UHV chamber the films have been covered with a Zr layer of 6.5 nm thickness (for the MOKE experiments) or 15 nm (for the x-ray experiments) to prevent oxidation of the $Fe_{100-x}Zr_x$ layer.

The samples have been characterized by x-ray diffraction and reflectivity measurements using Cu $K\alpha$ radiation in a Siemens D5000 with a Graphite monochromator in the diffracted beam under symmetrical Bragg-Brentano conditions. Magnetic properties have been characterized using an OXFORD vibrating sample magnetometer (VSM) with an applied field of up to 5 T. Magneto-optical Kerr effect (MOKE) measurements have been done using a wavelength $\lambda = 638$ nm *ex situ* in an applied field of up to 1 T perpendicular to the film surface. For *in situ* MOKE measurements, a field of 0.3 T perpendicular to the film surface was used. In both cases, polar MOKE has been measured using perpendicular incidence of the light. The structural state of the film surface during and after growth has been characterized by RHEED (reflection high-energy electron diffraction) using a 30 keV electron beam. To obtain a sufficient scattering intensity, a slightly divergent beam was used.

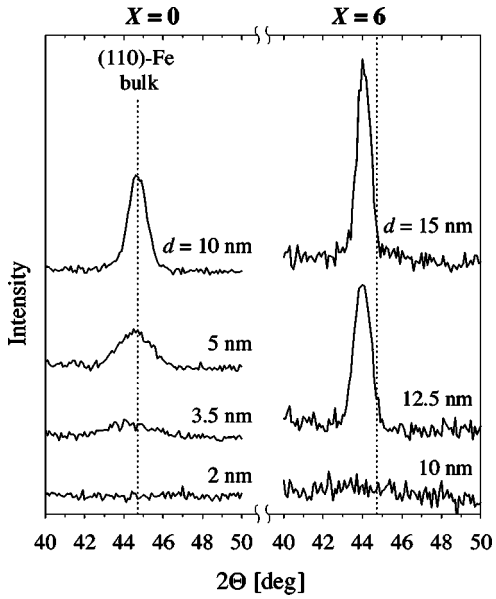

FIG. 2. X-ray diffraction patterns from the $Zr/Fe_{100-x}Zr_x/Zr$ samples with $x=0$ or $x=6$ for different thicknesses of the $Fe_{100-x}Zr_x$ layer as indicated.

III. RESULTS

A. X-ray diffraction

In Fig. 2, x-ray diffraction data from samples consisting of 30 nm Zr base layer, $Fe_{100-x}Zr_x$ layers with different thicknesses and a 15 nm Zr cover layer are shown for the compositions $x=0$ and $x=6$ at. % Zr. Below a critical thickness of 2 nm for $x=0$ or 10 nm for $x=6$, no Bragg peaks of the $Fe_{100-x}Zr_x$ layer can be detected. For the samples with larger $Fe_{100-x}Zr_x$ layer thickness, (110) Bragg reflections of the bcc structure are visible. This indicates that a transformation of the initially amorphous $Fe_{100-x}Zr_x$ layers to a bcc phase has taken place at the critical thickness. The thicknesses above which the bcc phase is observed vary from 2 nm for pure Fe to 10 nm for the 6 at.% Zr solid solution. The width of the peaks indicates coherence lengths perpendicular to the film surface which agree well with the nominal $Fe_{100-x}Zr_x$ layer thicknesses obtained from the quartz thickness monitors.

The Fe peaks are shifted from the theoretical positions for pure bcc Fe towards lower angles. The shift indicates the lattice expansion caused by the dissolved Zr. In addition, there is a significant contribution induced from the Zr substrate or the Zr-(Fe-Zr) interface. This contribution decreases with increasing layer thickness.[14] The lattice parameter of the alloy without the influence of the interfaces can be found by extrapolation to large layer thickness. The extrapolated values of the lattice parameters agree with those expected for a random bcc solid solution of Fe and Zr which have been calculated by linear interpolation between the atomic volumes of Fe and Zr (Vegard's law). The peak positions are therefore strong evidence for the polymorphous transformation of the initially amorphous layer into a bcc solid solution of Fe and Zr.

B. X-ray reflectivity

The density profiles of the samples have been investigated by x-ray reflectivity measurements. The measurements have

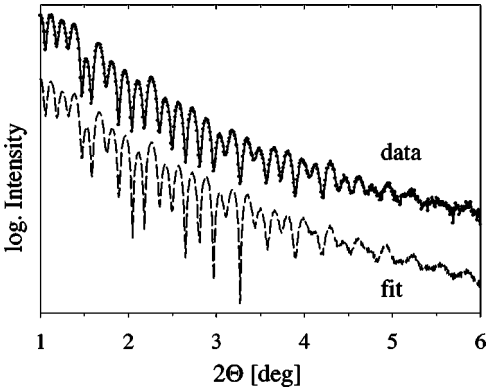

FIG. 3. Small angle x-ray scattering from the $Zr/Fe_{95}Zr_5/Zr$ sample with a 10 nm thick $Fe_{95}Zr_5$ layer. The dashed line is a fit using an optical model and has been shifted for better visibility.

been compared to theoretical curves calculated using an optical model.[15,16] As an example, Fig. 3 shows the x-ray reflectivity curve for Zr/Fe-Zr/Zr multilayer with a 10 nm thick layer of the composition $Fe_{95}Zr_5$ in comparison with the corresponding fit. The data show interference patterns due to the superposition of waves reflected at the surface and the internal interfaces of the films. To account for the decrease of the intensity with increasing scattering angle, a roughness of the interfaces and the surface has to be introduced in the model. From the fits of the data, one can extract the thicknesses of the individual layers and the roughness of the interfaces. The layer thicknesses are in good agreement with the nominal values from the quartz thickness monitors which are indicated in Fig. 3 in all cases. The values for the interface roughness are 0.3 nm for the SiO substrate surface, 0.6 nm for the interfaces between the $Fe_{95}Zr_5$ layer and the Zr base or top layer, and 0.77 nm for the surface of the top Zr layer. The specular reflectivity measurements cannot distinguish between roughness and interdiffusion of the components. It can be deduced, however, that no interdiffusion over more than a few interatomic distances can take place in the samples. This result has been further confirmed by Auger depth profiles obtained during ion beam etching of selected samples and Rutherford backscattering measurements.[14]

C. RHEED measurements

Selected samples have been studied by RHEED measurements during and after deposition under UHV conditions. In these studies, no Zr cover layer was present (see Fig. 1). The aim of the studies was to investigate the kinetics of the transformation to the crystalline state and the possible influence of the Zr cover layer. Using the divergent beam it was possible to obtain patterns from the polycrystalline or amorphous layers. The diffraction patterns obtained in this way resemble those obtained in an electron microscope. A series of diffraction patterns taken during a growth sequence of an $Fe_{94}Zr_6$ sample on top of a 30 nm Zr buffer layer is shown in Fig. 4. The diffraction pattern of the Zr buffer layer in Fig. 4(a) looks almost like a single crystal pattern. It is, however, invariant under rotation around an axis perpendicular to the film. From the pattern and this invariance it can be deduced that the Zr crystals in the buffer layer have a preferred orientation with (002) planes parallel to the film surface but no

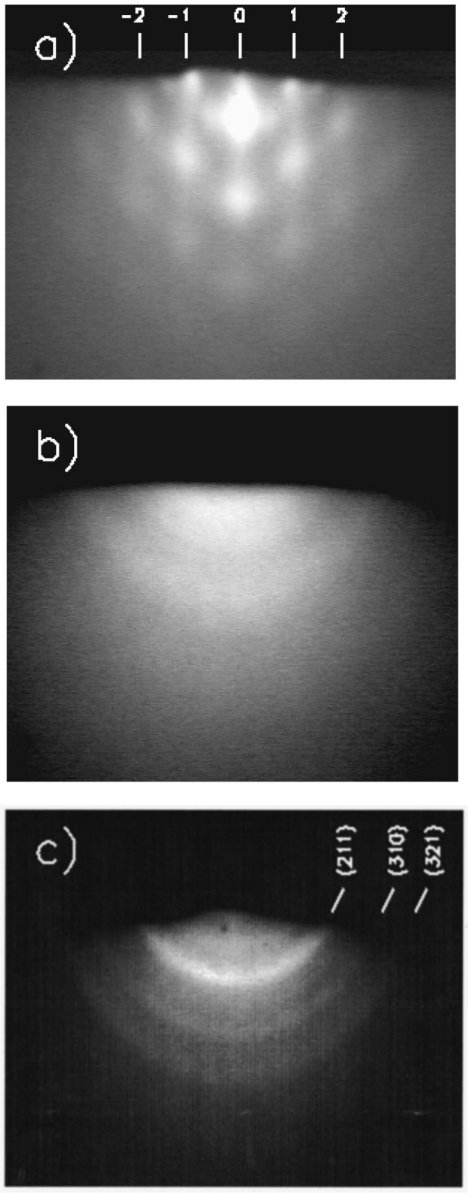

FIG. 4. RHEED patterns of the $Fe_{94}Zr_6$ growth sequence. The pictures are taken from the surface of the Zr buffer (a) and at 10 nm (b) or 15 nm (c) thickness of the $Fe_{94}Zr_6$ film.

preferred in-plane orientation. In Fig. 4(b), the Zr is covered by a 10 nm thick $Fe_{94}Zr_6$ layer. Only a broad diffuse pattern is observed. This diffuse pattern is already found at a coverage of less than 0.5 nm $Fe_{94}Zr_6$. The diffuse pattern remains until the critical thickness is reached and crystallization sets in. In Fig. 4(c), the diffraction pattern after deposition of 15 nm $Fe_{94}Zr_6$ on top of the Zr is shown. There are distinct diffraction rings visible now which can be attributed to the bcc $Fe_{94}Zr_6$ phase.

Since the RHEED measurements are surface sensitive, the results show that the surface of the $Fe_{94}Zr_6$ layers transforms into the crystalline state above a critical thickness. The critical thickness obtained in this way compares well with the critical thickness values above which Bragg peaks are visible in the XRD and ferromagnetism is detected. This result indicates that the Zr cover layer does not induce an additional phase transformation of the $Fe_{94}Zr_6$. The same result has been found for $x=0$, i.e., pure Fe layers.

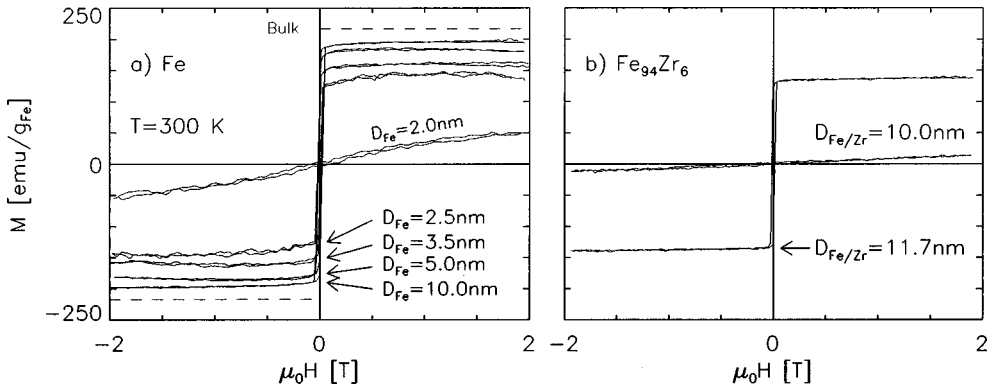

FIG. 5. Magnetization versus applied field measured at room temperature of the Zr/Fe$_{100-x}$Zr$_x$/Zr samples with (a) $x=0$ and (b) $x=6$.

In addition, RHEED measurements of a layer with a step profile have been done. To achieve the step profile, part of the substrate has been covered by a shutter during the first part of the deposition process. In this way, a subcritical and a supercritical part have been grown on the same Zr substrate layer in the covered or the open part, respectively. By moving the electron beam across the sample surface it was found that the thicker part of the layer shows a crystalline diffraction pattern as in Fig. 4(c) whereas the thin section remains amorphous.

D. Magnetic properties

As explained in the Introduction, the transition from the amorphous to the crystalline state can be verified by magnetization measurements. In Fig. 5, the magnetization curves vs applied field are shown for Zr concentrations of 0 to 6 at. %. The signal of the Si wafer substrates has been subtracted. The samples have been measured at room temperature where the amorphous Fe-rich phases are paramagnetic. The magnetization curves allow a quantitative determination of the amount of bcc phase present in the samples. It is observed from Fig. 5 that for each Zr concentration a transition from a paramagnetic to a ferromagnetic behavior occurs at a different thickness termed d_c afterwards.

A systematic evaluation of the dependence of the saturation magnetization on the thickness d of the Fe$_{100-x}$Zr$_x$ layers shows that the data can be described by a superposition of a ''magnetically dead'' (i.e., paramagnetic) layer of thickness d_{md} at the interfaces to the adjacent Zr layers and a ferromagnetic central part of the Fe$_{100-x}$Zr$_x$ layers. The thickness d_{md} may be calculated using the relation[17,18]

$$M_S(d_{\mathrm{Fe}})=M_S(d_{\mathrm{Fe}}\rightarrow\infty)\left(1-2\frac{d_{\mathrm{md}}}{d}\right). \qquad (1)$$

In Fig. 6, the magnetization values of the samples are drawn versus $1/d$. It is observed that the magnetization decreases proportional to $1/d$ as suggested by Eq. (1). The thicknesses d_{md} have been found to be about 0.5 nm for all Zr concentrations $x<6$. For the Fe$_{94}$Zr$_6$ layer, a thickness d_{md} of 1.1 nm has been calculated. The magnetization values $M_S(d_{\mathrm{Fe}}\rightarrow\infty)$ of the bulk Fe$_{100-x}$Zr$_x$ alloys show a continuous decrease from 217 emu/g$_{\mathrm{Fe}}$ to about 180 emu/g$_{\mathrm{Fe}}$ with increasing Zr concentration. The value of 217 emu/g for $x=0$ is in good agreement with the literature value for bulk Fe at room temperature.[19]

The values of d_{md} for the layers with $x<6$ at. % Zr are in good agreement with the interface roughness values deduced from the x-ray reflectivity measurements. The reason for the paramagnetic behavior of the interface layers seems to be the intermixing of Fe and Zr over 2–3 interatomic distances. The Zr-rich Fe-Zr alloy formed in this spatially confined region is paramagnetic at room temperature. The magnetization measurements show that the interface layers are not transformed back to the crystalline state as the remaining Fe$_{100-x}$Zr$_x$ layer.

E. MOKE measurements

As shown above, the magnetic properties of the amorphous and the crystalline phase make a quantitative evaluation of the phase fraction of the crystalline phase possible. This property has been used in magneto-optical Kerr effect (MOKE) studies of the Fe$_{100-x}$Zr$_x$ films.[20] The transition shows up as a jump in the MOKE rotation angle at a given applied field. This has been shown by MOKE measurements

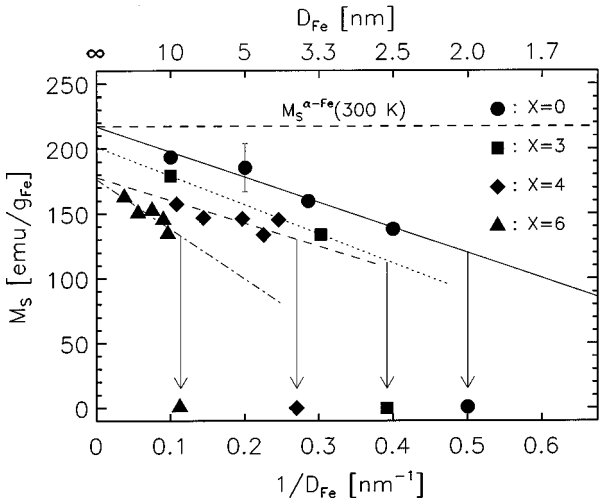

FIG. 6. Spontaneous magnetization of the Zr/Fe$_{100-x}$Zr$_x$/Zr samples for different Zr concentrations X (given in at. %) versus reciprocal Fe layer thickness $1/d_{\mathrm{Fe}}$. The dashed line marked $M_S^{\alpha\text{-Fe}}$ represents the literature value for bulk Fe.

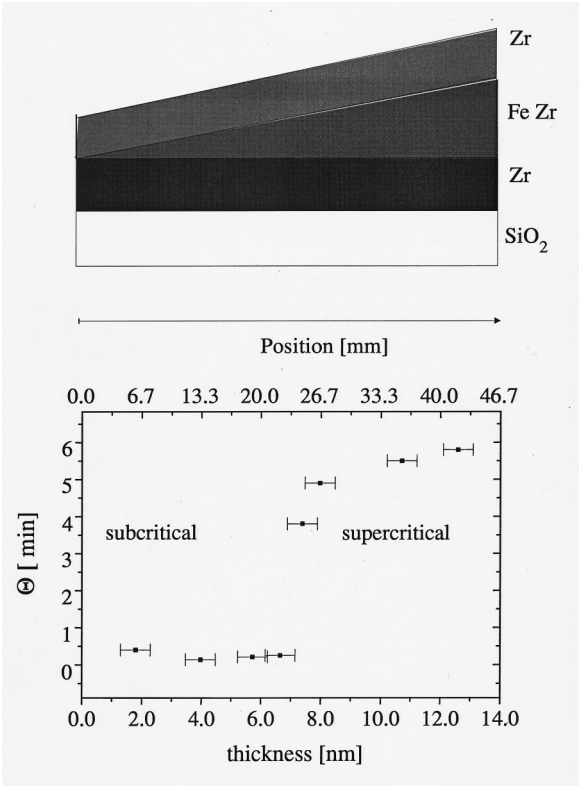

FIG. 7. Polar Kerr effect rotation angles of an $Fe_{94}Zr_6$ wedge shaped sample.

of samples with different thicknesses and composition. The results are illustrated in Fig. 7 which shows an *ex situ* MOKE measurement of an $Fe_{94}Zr_6$ wedge shaped layer at an applied field of 0.6 T. The wedge shape was obtained by continuously opening the substrate shutter during deposition. The thickness increases from zero at one end of the sample to about 14 nm at the opposite end. The maximum thickness has been determined from x-ray reflectivity measurements of a small piece cut from the sample. It is observed that a jump in the Kerr rotation of 4 min (0.067°) occurs at a thickness of about 8 nm. The further increase of the Kerr rotation with increasing layer thickness is mainly due to the influence of the demagnetization field of the samples under the measurement conditions used. The absolute value of the critical thickness of the jump cannot be determined with the same precision as in the other measurements since the thickness profile has not been determined in more detail. It is clear, however, that part of the layer below a critical thickness of $Fe_{94}Zr_6$ remains amorphous, whereas the part with a thickness above a critical value is crystalline.

IV. DISCUSSION

A. Model for the transformation

In this section, we will discuss a model for the crystallization of the $Fe_{100-x}Zr_x$ layers. The thermodynamic conditions in the Fe-Zr system and the stability of the metastable amorphous phase have been investigated previously using the CALPHAD method in Ref. 21. For $x<x_c\approx 8$ at.% a driving force $\Delta g_{c,a}$ for polymorphous (partitionless) crystallization exists. At the low temperatures under which the

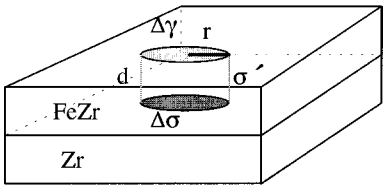

FIG. 8. Schematic model of a crystalline nucleus with radius r inside the amorphous thin film of thickness d. The interface energies considered are $\Delta\sigma$ between the nucleus and the Zr layer and σ' between the nucleus and the surrounding Fe-Zr layer. $\Delta\gamma$ is the contribution of the specific surface energy of the nucleus.

present experiments have been conducted, diffusion is slow so that alternative crystallization reactions requiring diffusive phase separation will not take place on the experimental time scale even if they would provide a larger energy gain.[22]

We consider now the possibility of homogeneous nucleation inside the layers. We use the relationship[22]

$$r_c=\frac{2\sigma' V^m}{\Delta g_{c,a}} \tag{2}$$

for the radius of the critical nucleus. Here, σ' is the specific energy per area of the interface between the crystalline nucleus and the amorphous phase and V^m is the molar volume. We may take a value of $\sigma'=0.28$ J/m^2,[23] which has been deduced from undercooling experiments. With that value we calculate $r_c=0.4$ nm from Eq. (2) using $\Delta g_{c,a}=10$ kJ/mol. (Ref. 21) for the pure Fe. The calculated r_c for pure Fe is on the order of the interatomic distance in Fe, so that the distinction between quenched in nuclei and thermally activated nucleation may no longer be appropriate. We do not have values of σ' for the $Fe_{100-x}Zr_x$ alloys with $x>0$, but since the driving force $\Delta g_{c,a}$ reduces with increasing Zr concentration x, we expect an increase of r_c with increasing x.

The experimental results show that the polymorphous crystallization of the initially amorphous $Fe_{100-x}Zr_x$ takes place at a concentration dependent critical thickness d_c. We will discuss here a model for the transformation of the amorphous $Fe_{100-x}Zr_x$ layer which is similar to the growth models for the martensitic transformation.[24,25] However, we will consider the special geometry of the thin films here. We assume that a nucleus of the crystalline phase does already exist. We further assume that the crystalline nucleus takes a disk shape during growth to minimize the interface to the remaining amorphous phase to which we attribute a positive interface energy σ'. The situation is drawn schematically in Fig. 8.

We can now write the energy change ΔG during the transformation of the disk shaped volume of radius r in a film of thickness d from the amorphous to the crystalline state:

$$\Delta G=\frac{\Delta g_{c,a}}{V^m}\pi r^2 d-\pi r^2(\Delta\sigma_{a,c}+\Delta\gamma_{a,c})+2\pi r d\sigma'. \tag{3}$$

The first term on the right of Eq. (3) is the energy gain associated with the transformation of the volume of the nucleus, the second and the third denote the energy neces-

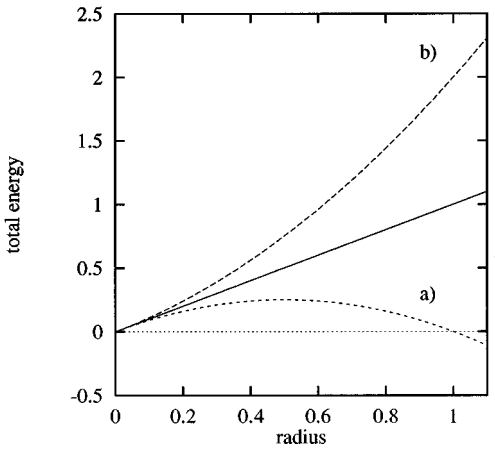

FIG. 9. Total free energy of a nucleus growing inside the $Fe_{100-x}Zr_x$ layer. Schematic curves for the cases where $\Delta g_{c,a}/V_m d-(\Delta\sigma_{a,c}+\Delta\gamma_{a,c})$ is (a) <0 or (b) >0 are shown. The solid line marks the boundary between the two regions.

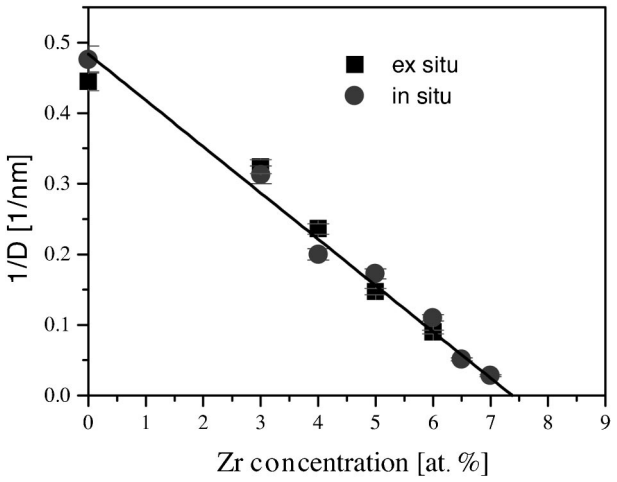

FIG. 10. Reciprocal critical thicknesses obtained by the *in situ* and *ex situ* measurements versus Zr concentration. The straight line represents a fit to the results according to Eq. (6).

sary to create the new interface to the Zr base layer or the surrounding $Fe_{100-x}Zr_x$ layer and the new surface. $\Delta\sigma_{a,c}$ is the difference between the interface energies of the amorphous or the crystalline $Fe_{100-x}Zr_x$ layer and the Zr substrate. $\Delta\gamma_{a,c}$ is the difference between the surface energies of the amorphous and the crystalline $Fe_{100-x}Zr_x$ layer. For simplicity, we assume that the molar volumes of the crystalline and the amorphous phase are equal. We only consider $x<x_c$ here so that $\Delta g_{c,a}<0$. We note that the stabilization of the amorphous phase by the interface energy difference requires $(\Delta\sigma_{a,c}+\Delta\gamma_{a,c})<0$ so that the second and the third term on the right side of Eq. (3) are positive.

In Fig. 9 the total free energies of the system versus the radius of the nucleus are drawn for different conditions. Since the first and the second term in Eq. (3) have the same functional dependence of r, we may distinguish two cases depending on whether $(\Delta g_{c,a}/V^m)d$ is less than or greater than $(\Delta\sigma_{a,c}+\Delta\gamma_{a,c})$. If the energy gain $(\Delta g_{c,a}/V^m)d$ cannot overcompensate $(\Delta\sigma_{a,c}+\Delta\gamma_{a,c})$, the total energy will always increase with increasing r [case (b) in Fig. 9]. In the other case, however, there exists a critical radius r^* above which the nucleus may grow with energy gain [case (a) in Fig. 9]. The necessary condition for the growth of the crystal nucleus is therefore

$$\frac{\Delta g_{c,a}}{V^m}d-(\Delta\sigma_{a,c}+\Delta\gamma_{a,c})<0. \tag{4}$$

B. Comparison with the experiments

The thermodynamic data of the Fe-Zr system[21] show that the driving force for polymorphous crystallization of amorphous Fe-rich Fe-Zr alloys into the bcc phase reduces continuously from about 10 kJ/mol for pure Fe to zero at the bulk stability limit $x_c\approx 8$ at. % Zr. We simplify by taking

$$\Delta g_{c,a}=g_c-g_a\approx\Delta g_0\left(1-\frac{x}{x_c}\right), \tag{5}$$

where Δg_0 is the difference of the molar free energy densities between crystalline and amorphous pure Fe and x_c is the stability limit of the bulk amorphous phase.

We may then express the condition for the fulfillment of Eq. (4) by a critical thickness d_c:

$$\frac{1}{d_c}=\frac{\Delta g_0}{V^m(\Delta\sigma_{a,c}+\Delta\gamma_{a,c})}\left(1-\frac{x}{x_c}\right). \tag{6}$$

We will verify now that Eq. (6) can describe the results of the experiments. For this purpose, we draw the reciprocal value of experimentally observed critical thicknesses d_c from both *in situ* and *ex situ* studies versus the Zr concentration. The result is shown in Fig. 10. It is seen that both *in situ* and *ex situ* measurements fall onto a common curve and are described by Eq. (6). As a result, we obtain x_c and the value of $(\Delta\sigma_{a,c}+\Delta\gamma_{a,c})$ if we take g_0 from the CALPHAD calculations[21] and V^m as the molar volume of Fe. The small ($<7\%$) variation of V^m with x due to the difference between the atomic volumes of Fe and Zr has been neglected. Note that we do not need the value of x_c from the CALPHAD calculations. The value derived from the fit is 7.4 at. % Zr. This is very close to both the CALPHAD calculations and the experimental findings from rapid quenching experiments.[13] The meaning of this value is that upon approaching the concentration x_c the critical thickness d_c diverges. Experimentally, the largest critical thickness observed here was about 30 nm for 7 at. % Zr (during the *in situ* Kerr measurements). Since the concentration can only be controlled to a limited precision, it would be difficult experimentally to approach the critical concentration further. The absolute value of the energy difference $|\Delta\sigma_{a,c}+\Delta\gamma_{a,c}|$ derived from the fit is 2.3 J/m^2.

It is clear from Fig. 10 that the simplified model can qualitatively describe the experimental results. We will now discuss the result more quantitatively. We start with an estimate of the individual interface energy contributions. Up to now, we have not included the effect of other energetic contributions, like elastic energy terms and defects. We will con-

sider the influences of these contributions on the transformation, especially on the value of $|\Delta\sigma_{a,c}+\Delta\gamma_{a,c}|$, in detail.

C. Consideration of individual energy contributions

1. Interface energy contributions

We will estimate the invidual energy contributions in Eq. (3) in detail now. The energy σ' represents the barrier against homogeneous nucleation of the crystalline phase inside the $Fe_{100-x}Zr_x$ layer. It is generally assumed that the energy of the crystal/amorphous interface is small in comparison with typical intercrystalline interfaces.[22] Often values of the crystal/liquid interface energies are used instead which are typically also <0.25 J/m^2.[26] As in the estimation of the homogeneous nucleation, we will take a value of $\sigma' \approx 0.28$ J/m^2 for the following discussion.[23]

The situation is more difficult for $\Delta\sigma_{a,c}$. The chemical part of the interface energy is neglected here since we assume the same values for the crystalline and the amorphous Fe-Zr layer and therefore no contribution to $\Delta\sigma_{a,c}$. We estimate the structural part of the interface energy between crystalline $Fe_{100-x}Zr_x$ and the crystalline Zr substrate layer from values for high angle grain boundaries to be of the order of 1 J/m^2. As already discussed, the interface energy between the amorphous $Fe_{100-x}Zr_x$ and the Zr substrate layer will be significantly lower and may be estimated to about 0.25 J/m^2. This will lead to a value of $\Delta\sigma_{a,c}$ of the order of -0.75 J/m^2.

The surface energy of the amorphous Fe is not known. We may again assume values from liquid Fe in view of the structural similarity between liquid and amorphous phase. A measured value for γ of liquid Fe is 1.8 J/m^2.[27] For the solid Fe (110) surface a surface energy of 2.08 J/m^2 has been measured.[28] We therefore expect that $\Delta\gamma_{a,c}$ falls into the range between -0.1 and -0.3 J/m^2.

These considerations show that the experimental value of $|\Delta\sigma_{a,c}+\Delta\gamma_{a,c}|$ is of similar magnitude as the values known for the individual contributions. However, the experimental value of 2.3 J/m^2 derived from the fit is larger than the sum of the estimated individual contributions which would be about 1 J/m^2. In the following, we will consider the influence of additional contributions on the value of $|\Delta\sigma_{a,c}+\Delta\gamma_{a,c}|$ determined from the experiments.

2. Elastic energy contributions

Two different elastic energy contributions may be present in our samples. First, there may be stress induced by the growth of the films which can lead to an energy contribution if the volume or the elastic properties of the layer change during the transformation. Second, a volume change during the transformation can lead to an elastic energy contribution even if there was no intrinsic stress before. Whereas the first contribution may increase or reduce the energy gained by the transformation depending on the sign of the stress and the volume change, the second contribution will always reduce the energy gain. Both contributions will shift the transformation to a different critical thickness for a given Zr concentration x and lead to a different apparent value of $|\Delta\sigma_{a,c}+\Delta\gamma_{a,c}|$. We will now try to estimate the magnitude of the effects.

In Co-Zr multilayer systems,[29] compressive stresses of 400–500 MPa have been measured during electron beam deposition at 523 K. Compressive stresses of the same magnitude have also been measured in Fe-Tb multilayers[30] grown by a face-to-face sputtering technique. We may estimate the stress contribution to the free energy density using[30]

$$\Delta g_s = p\Delta V^m = -\frac{2}{3}\sigma\Delta V^m. \tag{7}$$

Taking an in-plane stress σ of 500 MPa and an upper limit of 5% for the volume change during crystallization ΔV^m, we get only a contribution of about 0.2 kJ/mol to the total energy density.

We may estimate the second effect by assuming that the unconstrained layer would have a volume expansion $\Delta V = V_{bcc} - V_{am}$ which is afterwards compensated by a compression of the layer to its former area (which is fixed by the substrate). We can calculate the energy density for a polycrystalline Fe layer by

$$\Delta g = V^m \frac{E}{1-\nu}\epsilon_{xx}^2. \tag{8}$$

Here, E is the Young modulus of Fe [2.1×10^{11} Pa (Ref. 31)], ν is the Poisson number [0.287 (Ref. 31)], and ϵ_{xx} is the in-plane strain necessary to compensate the volume expansion. With a relative density change of 5% we get a value of Δg of about 0.5 kJ/mol. The transformation induced stress therefore seems to be more important than the stress built up during the layer growth.

We have observed that the interlayer spacing perpendicular to the surface of the crystalline $Fe_{100-x}Zr_x$ layers with $d>d_c$ is larger than the equilibrium value. For pure Fe layers, the observed magnitude of more than 2% would lead to a similar ϵ_{xx} via the relation[32]

$$\epsilon_{xx} = -\frac{1-\nu}{2\nu}\epsilon_{zz}. \tag{9}$$

However, the in-plane stress associated with the transformation would be several GPa. This is much more than the measured stress in the Fe-Tb multilayers.[30]

The volume change during crystallization of our amorphous $Fe_{100-x}Zr_x$ has not been measured up to now. Recently, the volume change during crystallization of the amorphous Fe layers in Fe/Gd and Fe/Y multilayers has been studied.[33,34] Within the experimental accuracy of about 2%, no difference between the density of the amorphous and the crystalline Fe was found.

We conclude here that the elastic energy effects are of minor importance in the presence of large driving forces Δg. For example, for the pure Fe the elastic energy effects would modify the driving force for the crystallization by less than 5% and, via Eq. (4), lead to the same relative change of $|\Delta\sigma_{a,c}+\Delta\gamma_{a,c}|$. We cannot exclude that they play a role close to x_c where the driving force for crystallization becomes smaller. For these concentrations, it might therefore also be possible to influence the transformation by the application of external stress in analogy to the so-called stress induced martensite.[25] This possibility is presently under investigation.[35] For systems where the driving force for the

transformation is smaller, elastic energies will have a more pronounced effect on the transformation than in the case studied here.

3. Grain boundary energy contribution

Another energy contribution may arise from defects inside the $Fe_{100-x}Zr_x$ layers. For the crystalline layer, one has to consider the contribution of grain boundaries which have an excess energy per area σ_{gb}. As mentioned before, the x-ray diffraction studies indicate that the grain size of the $Fe_{100-x}Zr_x$ crystallites in the direction perpendicular to the layer surface coincides with the layer thickness. However, the lateral grain size determining the grain boundary density in the layers after crystallization is not known. TEM cross section images of Fe-Zr multlayers with modulation periods of 8 nm (Ref. 36) or 9 nm (Ref. 37) and observations of Fe-Tb (Ref. 30) and Fe-Gd (Ref. 8) multilayers show that the lateral crystallite dimensions are larger than the Fe layer thickness. In Ref. 8, a lateral grain size d_l of 7 nm is measured at a Fe film thickness d of 3.2 nm. To estimate the effect, we assume $d_l = 2d$ and estimate the grain boundary contribution to the energy density g_{gb}:

$$g_{gb} \approx \frac{1}{2}\frac{\sigma_{gb} 2\pi d^2}{\pi d^3} = \frac{\sigma_{gb}}{d}. \tag{10}$$

For simplicity, we assumed a cylindrical grain shape here. The prefactor 1/2 is necessary to avoid counting of the grain boundary energy twice. The importance of this contribution depends on the value of σ_{gb}. If we assume random high angle boundaries, a value of $\sigma_{gb} \leqslant 1$ J/m^2 seems appropriate. This leads to a value of $g_{gb} \leqslant 3.5$ kJ/mol for the pure Fe layer at the critical thickness of 2 nm. The driving force for the crystallization will be reduced by σ_{gb}/d. The effect of grain boundaries will therefore have a significant effect on the determination of $|\Delta\sigma_{a,c} + \Delta\gamma_{a,c}|$ from the experiments. In particular, the grain boundary energy contribution may account for the difference between the experimentally determined value of 2.3 J/m^2 and the value of about 1 J/m^2 calculated from the estimated interface energies (see Sec. IV C 1). From the considerations given in this section, the value of $|\Delta\sigma_{a,c} + \Delta\gamma_{a,c}|$ after correction for grain boundary contributions would be lower by about 1 J/m^2, i.e., only about 1.3 J/m^2. This is much closer to the calculated value of about 1 J/m^2 than the value obtained without consideration of the grain boundary effect. The high density of grain boundaries may be a consequence of the large driving force for polymorphous crystallization of the Fe-Zr alloys in the concentration range studied here. The large driving force facilitates nucleation of the crystalline phase (see Sec. IV A) resulting in a high density of nuclei and a high density of grain boundaries in the crystallized layers. In other systems the density of nuclei may be smaller resulting in a lower density of grain boundaries and a less pronounced effect on the transformation.

V. CONCLUSION

The experiments presented in this work clearly demonstrate the balance between the effect of the stabilization of the amorphous Fe phase by the Zr substrate layer and the driving force for polymorphous crystallization in the $Fe_{1-x}Zr_x$ films. The polymorphous character of the transformation and the small effect of interdiffusion is clearly demonstrated. The transformation has been quantitatively characterized by the magnetic properties of the films. The condition for crystal growth obtained from the transformation model is compatible with all experimental observations and allows a quantitative determination of the stabilization effect as expressed by the difference between the interface energies of the competing phases. The contributions of elastic energy and defects may lead to an overestimation of the interface stabilization effect since they will reduce the available driving force for the transformation. For the polymorphous crystallization of the Fe-Zr studied here the driving forces are large. It is found that under these circumstances elastic energy contributions are less important, whereas the effect of grain boundaries has to be considered in a quantitative treatment. By taking into account the grain boundary effects, good agreement is obtained between the experimental results and calculations based on the individual interface energies. Since similar energetic contributions are present in other Fe–early transition metal or Fe–rare-earth multilayers, the effects found here should not be restricted to the Fe-Zr system but also apply to the other Fe multilayer systems. For transformations under smaller driving forces the elastic effects will be more important. The variation of the driving force for crystallization by the choice of the film composition offers new opportunities for the study of phase transformations in thin films.

ACKNOWLEDGMENTS

We acknowledge helpful discussions with F. Haider and M. Moske and the technical support of A. Spoerhase.

[1] C. L. Chien, S. H. Liou, and G. Xiao, in *Metallic Multilayers and Epitaxy*, edited by M. Hong, D. U. Gubser, and S. A. Wolf (TMS, Warrendale, 1988), p. 245.
[2] S. Mitani, A. Kida, and M. Matsui, J. Magn. Magn. Mater. **126**, 76 (1993).
[3] G. A. Prinz, Phys. Rev. Lett. **54**, 1051 (1985).
[4] S. Handschuh, J. Landes, U. Köbler, Ch. Sauer, G. Kisters, A. Fuss, and W. Zinn, J. Magn. Magn. Mater. **119**, 254 (1993).
[5] B. M. Clemens, J. Less-Common Met. **140**, 57 (1988).
[6] J. Thiele, F. Klose, A. Schurian, O. Schulte, W. Felsch, and O. Bremert, J. Magn. Magn. Mater. **119**, 141 (1993).
[7] R. Hassdorf, M. Arend, and W. Felsch, Phys. Rev. B **51**, 8715 (1995).
[8] J. Landes, C. Sauer, B. Kabius, and W. Zinn, Phys. Rev. B **44**, 8342 (1991).
[9] Y. Kozono, M. Komuro, S. Narishige, M. Hanazono, and Y. Sugita J. Appl. Phys. **63**, 3470 (1988).
[10] J. Q. Xiao, A. Gavrin, G. Xiao, J. R. Childress, W. A. Bryden, C. L. Chien, and A. S. Edelstein, J. Appl. Phys. **67**, 5388 (1990).
[11] K. Samwer, H. J. Fecht, and W. L. Johnson, in *Glassy Metals III*,

edited by H. Beck and H. J. Guentherodt (Springer, Berlin, 1994).
[12] K. M. Unruh and C. L. Chien, Phys. Rev. B **30**, 4968 (1984).
[13] Z. Altounian, E. Batalla, and J. O. Strom-Olsen, J. Appl. Phys. **59**, 2364 (1986).
[14] H. Geisler, *Augsburger Mathematisch-Naturwissenschaftliche Schriften 19* (Wissner, Augsburg, 1997).
[15] L. G. Parratt, Phys. Rev. **95**, 359 (1954).
[16] E. E. Fullerton, I. K. Schuller, H. Vanderstraeten, and Y. Bruynseraede, Phys. Rev. B **45**, 9292 (1992).
[17] T. J. Konno, T. Nakayama, B. M. Clemens, and R. Sinclair, in *Magnetic Ultrathin Films—Multilayers and Surfaces, Interfaces, and Characterization*, edited by B. T. Jonker *et al.*, MRS Symposia Proceedings No. 313 (Materials Research Society, Pittsburgh, 1993), p. 731.
[18] Z. S. Shan, S. Nafis, J. Woollam, S. H. Liou, and D. J. Sellmyer, J. Appl. Phys. **73**, 6347 (1993).
[19] B. D. Cullity, *Introduction to Magnetic Materials* (Addison-Wesley, Reading, MA, 1972).
[20] H. Ippach, Diploma thesis, University of Augsburg, 1997.
[21] F. Gaertner, C. Michaelsen, and R. Bormann, Philos. Mag. B **76**, 511 (1997).
[22] U. Koester and U. Herold, in *Glassy Metals I*, edited by H. J. Guentherodt and H. Beck (Springer, Berlin, 1981), p. 225.
[23] K. F. Kelton, in *Solid State Physics 45*, edited by H. Ehrenreich and D. Turnbull (Academic Press, San Diego, 1991), p. 75.
[24] M. Cohen and C. M. Wayman, in *Metallurgical Treatises*, Metallurgical Society, edited by J. Tien and J. Elliot (AIME, Warrendale, PA, 1981), p. 445.
[25] C. M. Wayman, in *Physical Metallurgy*, edited by R. Cahn and P. Haasen (Elsevier, Amsterdam, 1983), p. 1031.
[26] D. Turnbull, J. Appl. Phys. **21**, 1022 (1950).
[27] A. Zangwill, *Physics at Surfaces* (Cambridge University Press, Cambridge, England, 1988).
[28] H. Jones, Met. Sci. J. **5**, 15 (1971).
[29] M. Moske, Habilitationsschrift, University of Augsburg, 1997.
[30] T. Otto, Ph.D. thesis, University of Kassel, 1996.
[31] G. Simmons and H. Wang, *Single Crystal Elastic Constants and Calculated Aggregate Properties* (MIT Press, Cambridge, MA, 1971).
[32] L. D. Landau and E. M. Lifschitz, *Elastizitaetstheorie* (Akademie Verlag, Berlin, 1989).
[33] K. Pruegl, Ph.D. thesis, University of Regensburg, 1998.
[34] K. Pruegl and H. Hoffmann, in *Verhandlungen der Deutschen Physikalischen Gesellschaft (VI)*, Deutsche Physikalische Gesellschaft (Physikverlag, Weinheim, 1998), Vol. 33, p. 792.
[35] B. Koch, Diploma thesis, University of Augsburg, 1998.
[36] K. Yamamoto, T. Nakayama, H. Satoh, T. J. Konno, B. M. Clemens, D. A. Stevenson, R. Sinclair, and S. B. Hagstrom, J. Magn. Magn. Mater. **126**, 128 (1993).
[37] T. Nakayama, H. Satoh, T. J. Konno, B. M. Clemens, D. A. Stevenson, R. Sinclair, and S. B. Hagstrom, J. Magn. Magn. Mater. **126**, 105 (1993).